Role of gravity and capillary waves in the origin of circular hydraulic jumps

Hossein Askarizadeh [1,2] Hossein Ahmadikia,[2,*] Claas Ehrenpreis [1] Reinhold Kneer,[1]
Ahmadreza Pishevar,[3] and Wilko Rohlfs [1,†]

[1]*Institute of Heat and Mass Transfer, RWTH Aachen University, Augustinerbach 6, 52056 Aachen, Germany*
[2]*Department of Mechanical Engineering, University of Isfahan, 81746-73441 Isfahan, Iran*
[3]*Department of Mechanical Engineering, Isfahan University of Technology, 84156-83111 Isfahan, Iran*

In almost all of the studies on the circular hydraulic jump (CHJ), gravity had been considered as a significant variable that affects the formation of the jump. Most recently, gravity was deprived of being important in the origin of the CHJ, which challenged researchers in this field of fluid mechanics. This study addresses in detail the physical concepts behind this intriguing phenomenon occurring in the radial outspreading of a vertically downward free-surface liquid impinging jet upon a horizontal plate. The aim is to find out whether gravity plays any role in the origin of the CHJ. Accordingly, the jump evolution is investigated in two cases: first, the initial formation of the CHJ in which the subcritical flow downstream from the jump is approaching the outlet boundary (developing jump). Second, the final evolution of the CHJ in which a steady-state flow is circumventing an obstacle at the edge of the impinged plate and falling uniformly down from the outlet boundary (developed jump). The results indicate the existence of two different flow regimes in the jump formation: gravity- and capillary-dominant flow regimes. In general, the role of gravity in the formation of developing or developed jumps cannot be eliminated; however, its importance lies in the fact of which regime dominates the flow. Intensification of gravitational effects is observed when capillary waves are dampened by increasing viscosity, density, or volume flow rate as well as by decreasing surface tension. Finally, a generalized scaling relation for the jump radius is obtained considering both capillary and gravitational effects in the critical flow condition. In contrast to the previous results, this generalized scaling relation predicts more accurately the radius of both a developing and a developed jump.

I. INTRODUCTION

Instantaneous changes in fluid flows bring many complexities into the analysis and assessment of the flow. One of the well-known examples of such a state is the transition between super- and subcritical free-surface liquid flows, where the occurrence of flow separations and counterrotating vortices in the hydraulic jump region causes difficulties in characterizing the flow, apart from mathematical complexities in solving elliptical equations for subcritical flows.

A circular hydraulic jump (CHJ) is a very common phenomenon and can be simply observed in everyday life, such as in an empty sink, when a round vertical liquid jet impinges upon a horizontal plate and spreads radially out in a thin film along the plate. Close to the stagnation point, the film thickness first reduces due to the acceleration of the flow and subsequently begins to gradually

---

*Corresponding author: ahmadikia@eng.ui.ac.ir
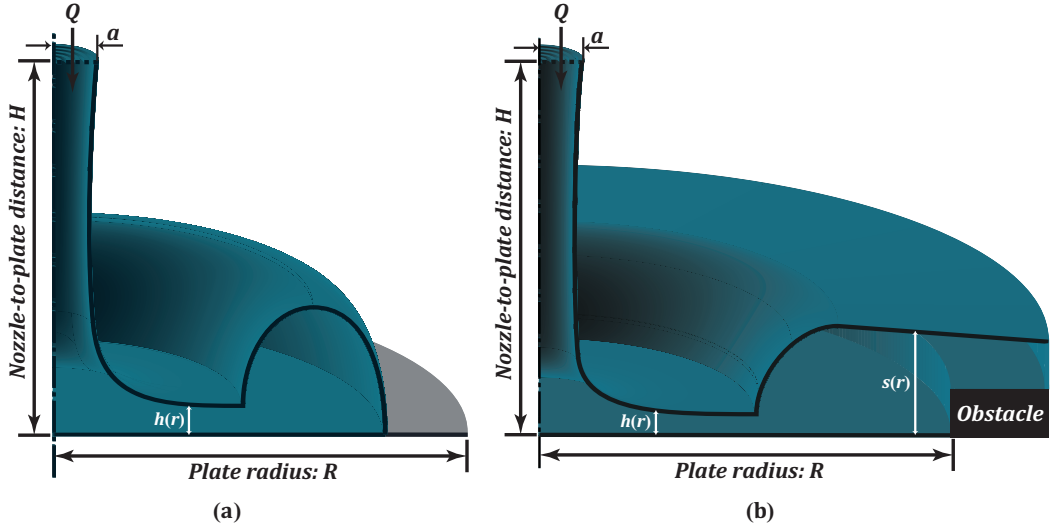†Corresponding author: rohlfs@wsa.rwth-aachen.de

FIG. 1. Formation of a CHJ before and after the arrival of the flow at the outlet boundary. (a) Developing CHJ. (b) Developed CHJ.

increase as a result of drag forces up to the jump position, where a sudden change in the flow thickness occurs. This intriguing phenomenon has been the subject of numerous studies. The first effort for describing the nature of hydraulic jumps is attributed to Leonardo da Vinci [1]. Despite the rich history of scientific research in this field, the origin of hydraulic jumps is still investigated in the fluid mechanics community. Most recently, the study of Bhagat *et al.* [2] has challenged researchers in the field to the question of whether gravity plays any role in the occurrence of the CHJ. Assigning an insignificant role to gravity in the origin of the CHJ questions the results of more than a century of scientific research in this field.

The idea of depriving gravity of being important in the origin of CHJs has been raised by Bhagat *et al.* [2], because they observed that the orientation of a jet—a vertical impinging jet on a horizontal plate either from above or from below, or the impingement of a similar but horizontal jet on a vertical plate—does not change the position of the jump, as long as the subcritical flow after the jump has not yet reached the outlet boundary. The initial formation of a CHJ, in which the flow downstream of the jump has not yet arrived at the outlet boundary, is hereafter called a *developing jump* [Fig. 1(a)]. Once the flow downstream of the jump arrives at the outlet boundary, transport of information takes place from the outlet boundary toward the jump, which considerably affects the final formation of a CHJ. The steady-state CHJ, in which the flow downstream of the jump falls uniformly down from the outlet boundary, is hereafter called a *developed jump* [Fig. 1(b)].

Gravity, however, was considered as a main parameter defining the CHJ position in the well-known studies of Watson [3] and Bohr *et al.* [4], who presented the following correlations for the jump radius, respectively:

$$\frac{R_j d^2 g a^2}{Q^2} + \frac{a^2}{2\pi^2 R_j d} = \begin{cases} 0.10132 - 0.1297\left(\frac{R_j}{a}\right)^{\frac{3}{2}}\mathrm{Re}^{-\frac{1}{2}} & R_j < r_0, \\ 0.01676\left[\left(\frac{R_j}{a}\right)^3 \mathrm{Re}^{-1} + 0.1826\right]^{-1} & R_j \geqslant r_0, \end{cases} \tag{1}$$

$$R_j \sim (q^5 \nu^{-3} g^{-1})^{1/8}, \quad q = \frac{Q}{2\pi}. \tag{2}$$

In the above equations, R_j denotes the jump radius, d the downstream height, g the gravitational acceleration, a the nozzle radius, Q the volume flow rate, Re the Reynolds number, ν the kinematic viscosity, and r_0 the radial position where the thickness of the boundary layer reaches the free surface $r_0 \approx 0.3155\, a\, \mathrm{Re}^{\frac{1}{3}}$ [3]. Watson's model, Eq. (1), requires experimental information on the

downstream height to evaluate the jump position, and the scaling relation of Bohr *et al.* [4], Eq. (2), has been criticized for excluding the effects of surface tension, density, and downstream height on the jump [5,6].

Liu and Lienhard [7] reviewed the studies that had evaluated Watson's model and explained the reasons for its inaccuracy in supercritical high-Froude number flows and in cases having a high downstream flow height in comparison to that of the upstream. In accordance with Ref. [7], Bush and Aristoff [8] incorporated surface tension effects into Watson's theory to improve its accuracy for predicting the hydraulic jump radius. They showed that their correlation is in a slightly better agreement with experimental results in comparison to that of Watson. However, they left the investigation of the influences of surface tension gradients on the jump position for future consideration owing to its complications. Mohajer and Li [9] showed that Watson's theoretical results can be successfully applied to develop a theory for CHJs with a capillary limit, in which the outer film is bounded by a stable rim and the contact angle considerably affects the jump. In accordance with the experimental observations, they showed that jump radius varies linearly with the flow rate in these kinds of problems and the surface tension controls the slope of this linear variation. Fernandez-Feria *et al.* [10] showed that the flow downstream of the developed jump depends significantly on the surface tension and downstream boundary condition. They found a critical value for the surface tension (σ^*) in the range of $0.025\sigma_w < \sigma^* < 0.05\sigma_w$ (σ_w is the surface tension of water), above which a stationary jump no longer exists.

The scaling relation of Bohr *et al.* [4], Eq. (2), was developed based on the theoretical model of Tani [11] and Kurihara [12], who mainly studied the fully viscous sheet flow on an impinged plate by a simple generalization of the shallow water theory. Accordingly, Bohr *et al.* [4] employed the mean value approach to average the boundary layer equations over the flow thickness and applied a parabolic velocity profile. They found that volume flow rate and viscosity strongly affect the jump position and presented the scaling relation in Eq. (2). They later modified this approach including a shape parameter in the velocity profile that makes the theory capable of treating the separation region of the jump as well [13]. Using this theory, Watanabe *et al.* [14] obtained a system of two ordinary differential equations describing the jump. Their solution shows that the hydraulic jump problem with a separation bubble on the bottom surface can be properly solved. However, the absence of the effects of surface tension forces and dynamic pressure variations in the theory of Bohr *et al.* [13] was questioned by Yokoi and Xiao [15,5]. In accordance with Ref. [7], Yokoi and Xiao [15,5] argued that transitions between jump structures are caused by the counteraction between surface tension forces, which are due to the curvature in the jump region, and relatively high dynamic pressure gradient zones, which occur underneath the interface in the jump region. The lack of surface tension, downstream height, and density effects in the scaling relation of Eq. (2) was also questioned in Ref. [6]. Rojas *et al.* [6] numerically solved the CHJ based on the inertial lubrication theory and derived the following scaling relation, which includes the downstream height (*s*) and shows accurate results at low and high Reynolds number flows, corroborating earlier findings [4,16–18]:

$$R_j \sim (q^3 \nu^{-1} g^{-1} s^{-2})^{1/4}. \tag{3}$$

A simple model was recently developed by Wang and Khayat [19] that predicts the radius and height of developed jumps for high-viscous liquid jets. The model explores effects of gravity on the supercritical flow upstream of the jump and shows that if gravity is included, the location of the jump will coincide with the singularity in the jump region, where the flow is separated. An important advantage of this model is that the jump position can be determined in high-viscous liquid jets without any knowledge of downstream flow conditions.

None of the studies, mentioned above, considered a developing CHJ, i.e., before the flow reaches the outlet boundary, which has been recently investigated by Bhagat *et al.* [2]. They presented a theory by introducing an energy equation that includes the flux of surface energy and leads to a new critical flow condition $\mathrm{We}^{-1} + \mathrm{Fr}^{-2} = 1$ for the jump position. This theory has been just recently criticized by Duchesne *et al.* [20], showing that such a condition (actually, $\alpha^2 \mathrm{We}^{-1} + \mathrm{Fr}^{-2} = 1$, where $\alpha = h/r$ is the aspect ratio of radial variations of the flow thickness over the radius) can at

best predict an upper bound on the jump radius. This problem apart, Bhagat *et al.* [2] found the significant role of the density (ρ) as well as surface tension (σ) in the scaling of a developing jump instead of the role of gravity as follows:

$$R_j \sim (q^3 \rho \nu^{-1} \sigma^{-1})^{1/4}. \tag{4}$$

In this study, a developing CHJ as well as a developed one are scrutinized in order to distinguish the dominant parameters in the formation of a CHJ and also to find out to which extent the claim of Bhagat *et al.* [2] for depriving the role of gravity in the origin of CHJs is applicable. Accordingly, the presence of two kinds of flow regimes is indicated: gravity- and capillary-dominant regimes. When capillary effects dominate the flow, gravity shows a negligible effect on the formation of the jump. On the other hand, when gravitational effects dominate the flow, the significant role of gravity in the origin of CHJs is depicted, which clarifies that the claim of Bhagat *et al.* [2] is not unconditionally true. Hence, it is shown that predictions of the scaling relation of Bhagat *et al.* [2], Eq. (4), can noticeably deviate from the jump position in gravity-dominated flow regimes. Furthermore, it is clarified how the variation of other parameters such as the volume flow rate, density and viscosity affects the formation of a CHJ in capillary- and gravity-dominated regimes. Eventually, the scaling analysis of Bhagat *et al.* [2] is modified to obtain a generalized scaling relation for the jump position, which includes both gravity and capillary effects. For these purposes, the applied numerical method and the governing equations together with the proof of the numerical accuracy are presented in Sec. II, and Sec. III depicts the contribution of the important parameters to the formation of CHJs.

II. NUMERICAL METHODOLOGY

A. Governing equations

Under the assumption of a laminar free-surface radial flow, fully incompressible two-phase Navier-Stokes equations applying the volume of fluid (VOF) method [21] can be written out using the Einstein summation convention for continuity, momentum, and volume fraction (α), respectively as follows:

$$\frac{\partial u_i}{\partial x_i} = 0, \tag{5}$$

$$\frac{\partial \rho u_i}{\partial t} + u_j \frac{\partial \rho u_i}{\partial x_j} = -\frac{\partial p}{\partial x_i} + \nu \frac{\partial^2 \rho u_i}{\partial x_j \partial x_j} + f_i^\sigma + f_i^g, \tag{6}$$

$$\frac{\partial \alpha}{\partial t} + \frac{\partial \alpha u_i}{\partial x_i} = 0. \tag{7}$$

To incorporate surface tension forces, $\mathbf{f}^\sigma$ (σ stands for the surface tension), the continuum surface tension model [22] is applied in which the surface curvature, $\vec{\kappa}$, is estimated through the following second derivative of the volume fraction field (α):

$$\mathbf{f}^\sigma = \sigma \kappa \hat{n} = -\sigma (\nabla \cdot \hat{n}) \hat{n}, \quad \hat{n} = \frac{\nabla \alpha}{|\nabla \alpha|}. \tag{8}$$

Note that the surface tension force has two components and is modeled through a continuum surface force method in a VOF analysis. The first component is due to the local curvature and is normal to the interface. The second one is due to local variations of the surface tension coefficient and is tangential to the interface. In the VOF approach, a continuous volume force, which applies to fluid elements everywhere within a thin transition region near the interface, replaces the surface force localized at the fluid interface. The continuum surface force method removes topological restrictions without losing accuracy [22], and it has thus been widely and successfully used in a variety of studies [23–26].

Under the application of the VOF method, the phase fraction values are used in the following manner to calculate any required property, χ, for the mixed fluid of liquid (l) and gas (g):

$$\chi = \alpha \chi_l + (1 - \alpha) \chi_g. \tag{9}$$

The open field operation and manipulation library (OpenFOAM) [27–29] is used to solve the jet flow under the interFoam solver, a finite-volume implementation of the VOF method [21]. It models multifluid flows by the cell-average volume fractions of the secondary phase. The free-surface flow of two immiscible and incompressible fluids is numerically calculated by solving the advection of the volume fractions and the fully resolved Navier-Stokes equations for mass and momentum.

As the finite-volume discretization defines cell-average volume fractions, the interface is represented by mixed cells that contain both fluids. To avoid numerical diffusion of the interface, interFoam introduces an artificial antidiffusive flux in the direction normal to the interface, known as the interface compression method. In capillary-dominated flows, interfacial forces must be obtained from the curvature of the interface. If the exact interface location is not required, interface curvature can be reconstructed from the divergence of the interface normal vector using vector field calculus, which is implemented in the interFoam solver. The resulting interfacial forces are converted into cell-average volume forces by the continuum surface force method [22].

Because of the accuracy limitations inherent to the interFoam solver [30], the interface compression scheme is amended by a limiter to avoid artificial oversharpening of the interface, and interfacial forces are calculated by the continuum surface stress method [31]. This variant of interFoam has the following advantages over its original. First, capillary pressures are predicted correctly. Second, predictions do not depend on the strength of the antidiffusive flux. Third, predictions are independent on the frame of reference that is crucial to calculations of traveling waves in liquid films and leads to steady-state problems in a frame of reference moving at the phase velocity. A detailed description of the model together with its validation is given in Rohlfs and Pischke [32]. In addition, validation of the model has been shown for falling liquid films by Rohlfs *et al.* [33], and it is shown for CHJs in Sec. II B.

B. Verification and validation

The numerical procedure is similar to the approaches described in Refs. [33–36]. Figures 2(a) and 2(b) show the computational domain and the boundary conditions as well as the qualitative distribution of the grid cells. The wall group with the no-slip condition consists of the impinged plate, obstacle (provided that a developed CHJ is under consideration), and upper wall, which is related to outer diameter of the nozzle. The dimensionless height and length of the obstacle are $\zeta_o = h_o/D = 0.2$ and $\xi_o = l_o/D = 2$ (D is the nozzle diameter), respectively. It should be noted that the obstacle is used only for the simulation of developed jumps. For the surrounding condition where the pressure is specified and either an inflow or an outflow may occur, a velocity inlet/outlet boundary condition is applied, in which the patch normal velocity is calculated according to the pressure gradient. At the inlet, a fully developed parabolic velocity profile in conjunction with the static atmospheric pressure is imposed. The spatial derivatives are discretized using a central difference scheme and the temporal ones by a first-order bounded implicit scheme.

In order to verify the independence of the numerical results from the used grid, in which the grid cells are uniformly distributed in both directions, two aspects have been inspected; the dependence of the wall gradient and that of the interface profile on the grid resolution. Figures 3 and 4 present the suitability of the grid resolution for further computations with a dimensionless cell size $\Delta \xi = \Delta r/D = \Delta \zeta = \Delta z/D = 5.0 \times 10^{-3}$, where ξ and ζ are the dimensionless radial and axial coordinates, respectively. The presented interface profiles in Fig. 3(a) and the wall gradient in Fig. 4(a) result from the simulation of a flow that is approaching the outlet, i.e., a developing jump, at the dimensionless time $\tau = t\nu/D^2 = 8 \times 10^{-2}$. The variations of wall gradient and interface profiles in the jump region are magnified in the insets of these figures. At the contact point of the liquid, gas, and plate, the application of zero gradient boundary condition for volume
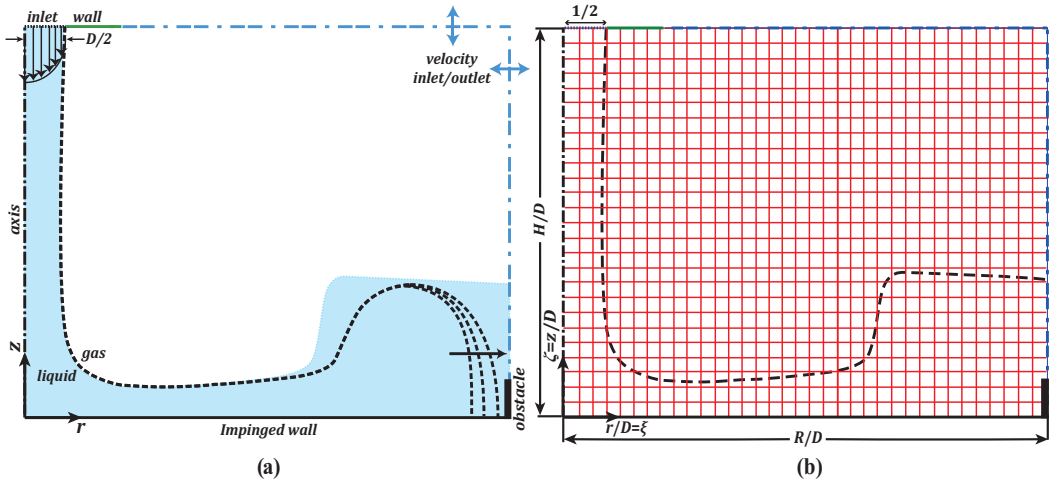
FIG. 2. (a) Computational domain with the boundary conditions; dashed lines schematically show an initial formation of the jump before the flow reaches the outlet boundary (a developing jump) and the light blue background segment illustrates a steady-state flow dropping down from the outlet (a developed jump) (b) Qualitative grid cells distribution and the dimensionless length scales based on the nozzle diameter.

fraction provides a 90° contact angle. At this point, a sudden variation of the wall gradient due to the discontinuity is expected, which is enlarged in Fig. 4(a). It should be kept in mind that the contact angle would expectedly affect the developing jump [38,39]. However, Bhagat *et al.* [2] experimentally found that there is a very small difference between the jump positions forming on the glass (hydrophilic) and Teflon (hydrophibic) surfaces. Therefore, the effects of the contact angle are not investigated in this study, which restricts the results to a constant contact angle.

Figure 3(b) shows that the grid resolution is fine enough to be applicable for the steady-state flow over the obstacle (developed jump) as well. It should be noted that the presented grid study has been done for the dimensionless nozzle-to-plate distance $H/D = 2$ and the dimensionless plate radius $R/D = 8$ in conjunction with the entrance Reynolds, $\mathrm{Re}_i = 4Q/\nu\pi D = 764$, Weber, $\mathrm{We}_i = \mathrm{Re}_i^2 \, \rho \, v^2/\sigma D = 288$, and Froude, $\mathrm{Fr}_i = 4Q/(\pi D^2 \sqrt{gD}) = 9.756$, numbers. This configuration has
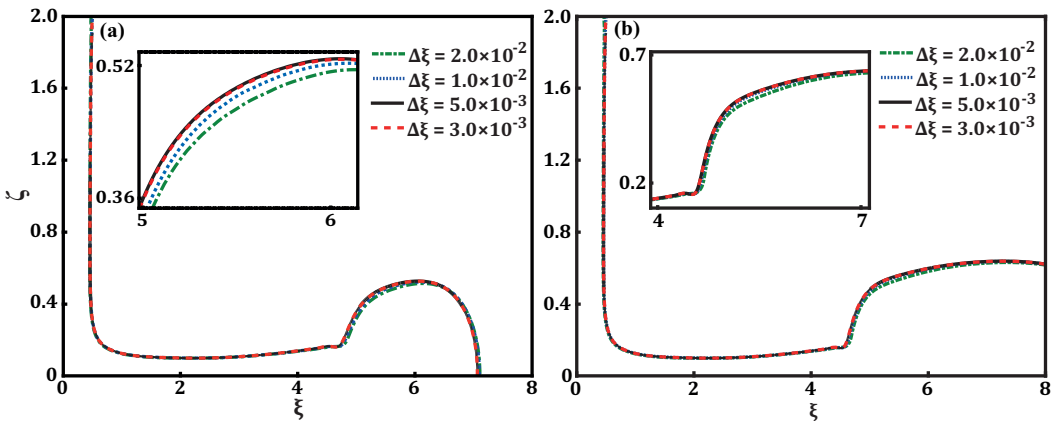

FIG. 3. Independence of the interface profile from the grid resolution: (a) Flow approaching the outlet boundary at $\tau = 8 \times 10^{-2}$; (b) final evolution of the flow over the obstacle.
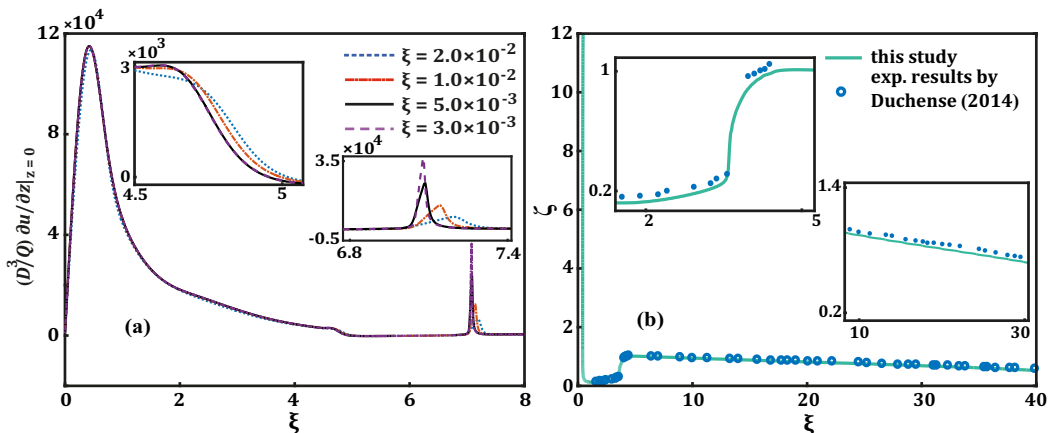
FIG. 4. (a) Independence of the wall gradient from the grid resolution. (b) Comparison with the experimental study by Duchesne et al. [37].

been used for all the studied cases in this paper. However, the grid resolution was also checked for the cases with the highest entrance Reynolds, Weber, and Froude numbers presented in this study, showing the trustworthiness of the used grid in the range $Re_i < 1.186 \times 10^3$, $We_i < 1.296 \times 10^3$, $Fr_i < 13.798$.

To validate the results of the computational scheme, a comparison with the experimental study of Duchesne [37] on the impingement of a laminar oil jet is presented in Fig. 4(b). The authors thank Prof. T. Bohr for sharing the relevant experimental results with us. The numerical results are in good agreement with the jump radius and the up- and downstream heights of the flow. The working fluid is silicon oil at room temperature ($\nu = 20$ cSt, $\sigma = 20$ mN m^{-1}, and $\rho = 0.96$ g cm^{-3}) that is released from a circular nozzle with a diameter of 3.2 mm as a developed flow. Hence, a parabolic entrance velocity profile is applied for the simulation. The volume flow rate is 17 cm^3 s^{-1} and the flow passes through a 4 cm nozzle-to-plate distance to impinge on a circular plate with the diameter of 30 cm and without any obstacle at the edge of the plate.

III. RESULTS AND DISCUSSIONS

The results chapter is divided into three sections. First, the question raised by Bhagat et al. [2] is addressed whether and to which extent gravity influences the initial formation of a CHJ (a developing jump). Further, the influence of the most important parameters on the formation and positioning of a CHJ is addressed. Finally, a generalized scaling analysis for the jump radius is presented.

A. Gravity- versus capillary-dominated developing CHJs

Gravity-dominated free-surface flows, such as open channel flows, exhibit sub- and supercritical flow behavior based on the ratio between flow velocity and wave velocity. In the supercritical state, the flow velocity exceeds the wave velocity, such that the transport of information is downstream only. The Froude number, which can be seen as the ratio between the flow velocity and the gravity waves velocity, is the relevant dimensionless number. In the subcritical state, the Froude number is less than one. The distinction between sub- and supercritical flow behaviors is also relevant for a CHJ to determine the jump position [3,4]. The corresponding local variation of the Froude number is $Fr(r) = Q/2\pi r h(r) \sqrt{g h(r)}$, where $h(r)$ is the radial variation of the flow thickness.

For a CHJ, however, the small length scales of the wall jet (flow thickness) prior to the appearance of the jump suggest that capillary forces and waves could be of significance as well. The critical

wave velocity to distinguish between sub- and supercritical flow conditions is thus also the capillary wave velocity, not only the gravity waves velocity. In the subcritical state, capillary waves can travel towards the stagnation point, in the opposite direction of the flow velocity. The local variation of the Weber number, $We(r) = \rho Q^2/4\pi^2 r^2 \sigma h(r)$, is the relevant parameter to estimate capillary effects.

In this regard and to comprehend the origin of CHJs, it is necessary to clarify whether the speed of the transport of information by capillary waves and/or by gravity waves exceeds the flow velocity to distinguish between super- and subcritical flows. The superposition of both mechanisms hinders in most cases a clear distinction. The presented theory by Bhagat *et al.* [2] introduces a new critical flow condition, $Fr^{-2} + We^{-1} = 1$, in which the roles of both capillary and gravity waves are taken into account. This condition is further investigated here.

Figure 5 presents the numerical simulation results for two different developing CHJs. The flow conditions are summarized in Table I. The surface tension is chosen such that the developing jump is significantly affected by gravitational forces on the left side while it is essentially affected by capillary forces on the right side. The evolution of the interface geometry shown in the top row is in accordance with the observations of Bhagat *et al.* [2] on a fixed position of the jump before the flow reaches the outlet boundary. However, an increased surface tension (right side) delays the arrival of the flow at the outlet boundary by increasing the downstream height [Fig. 5(a2)]. This is the result of higher capillary forces that cause a droplet-shape fluid bulb downstream of the jump. The deeper fluid flow downstream of the jump reinforces hydrostatic pressure acting against momentum and slightly shifts the jump position upstream.

To distinguish between the role of gravitational and capillary forces, various criteria for the location of the hydraulic jump are compared in the second and third rows of Fig. 5. A phenomenological characteristic is the location of the highest interfacial gradient, dh/dr [15]. To identify the role of gravitational and capillary waves, variations of the inverse Weber number and the Froude number squared as well as their combination $Fr^{-2} + We^{-1}$ are plotted.

For a gravity-dominated CHJ (left side), the inverse Weber number is significantly below unity [Fig. 5(b1)]. In contrast, the inverse Froude number squared quickly increases near the location of the hydraulic jump and surpasses unity. Due to the small effect of the Weber number, the combination of the Froude and Weber numbers ($Fr^{-2} + We^{-1}$) surpasses unity slightly upstream. Note that the highest interfacial gradient is very close to the location defined by $Fr = 1$.

For a capillary-dominated CHJ (right side), the inverse Weber number surpasses unity upstream of the location where the inverse of the Froude number squared surpasses the value of unity [Fig. 5(b2)]. Both courses, Fr^{-2} and We^{-1}, increase significantly downstream of the hydraulic jump. However, at the location defined by $Fr^{-2} + We^{-1} = 1$ the inverse Weber number dominates. Figure 5(c2) shows the surface geometry that exhibits a significant capillary wave before the hydraulic jump. The highest interfacial gradient is also close to the location defined by $We = 1$.

Therefore, the claim of Bhagat *et al.* [2] for neglecting gravitational effects on developing jumps and being content with $We = 1$ as the critical flow condition to obtain the position of a developing jump does not hold up in gravity-dominated flow regimes. In other words, the traditional way of demarcating between sub- and supercritical flows, $Fr = 1$, is quite accurate in gravity-dominated flow regimes for developing jumps.

Accordingly, it is expected that the scaling relation presented by Bhagat *et al.* [2], Eq. (4), does not work well in gravity-dominated flow regimes. To show this, Fig. 6(a) compares the locations of developing CHJs on the basis of the condition of $Fr^{-2} + We^{-1} = 1$ with those on the basis of Eq. (4) for a broad variation of the surface tension, which includes the transition between capillary- and gravity-dominated flow regimes. In this case, the transition occurs around $\sigma \approx 0.03$ N m^{-1}. For high capillary forces ($\sigma > 0.03$ N m^{-1}), good agreement is observed. However, for low capillary forces ($\sigma < 0.03$ N m^{-1}), predictions of Eq. (4) noticeably deviate from the jump position owing to the increasing significance of gravitational effects. For $\sigma = 0.01$ N m^{-1}, the error of Eq. (4) in predicting the jump position is about 27%. In capillary-dominant flow regimes, however, the jump positions are well captured, applying a constant coefficient $c = 0.262$ [which is needed in Eq. (4); see Fig. 6(a) as well] instead of the theoretical (0.277) and experimental (0.289) values reported by
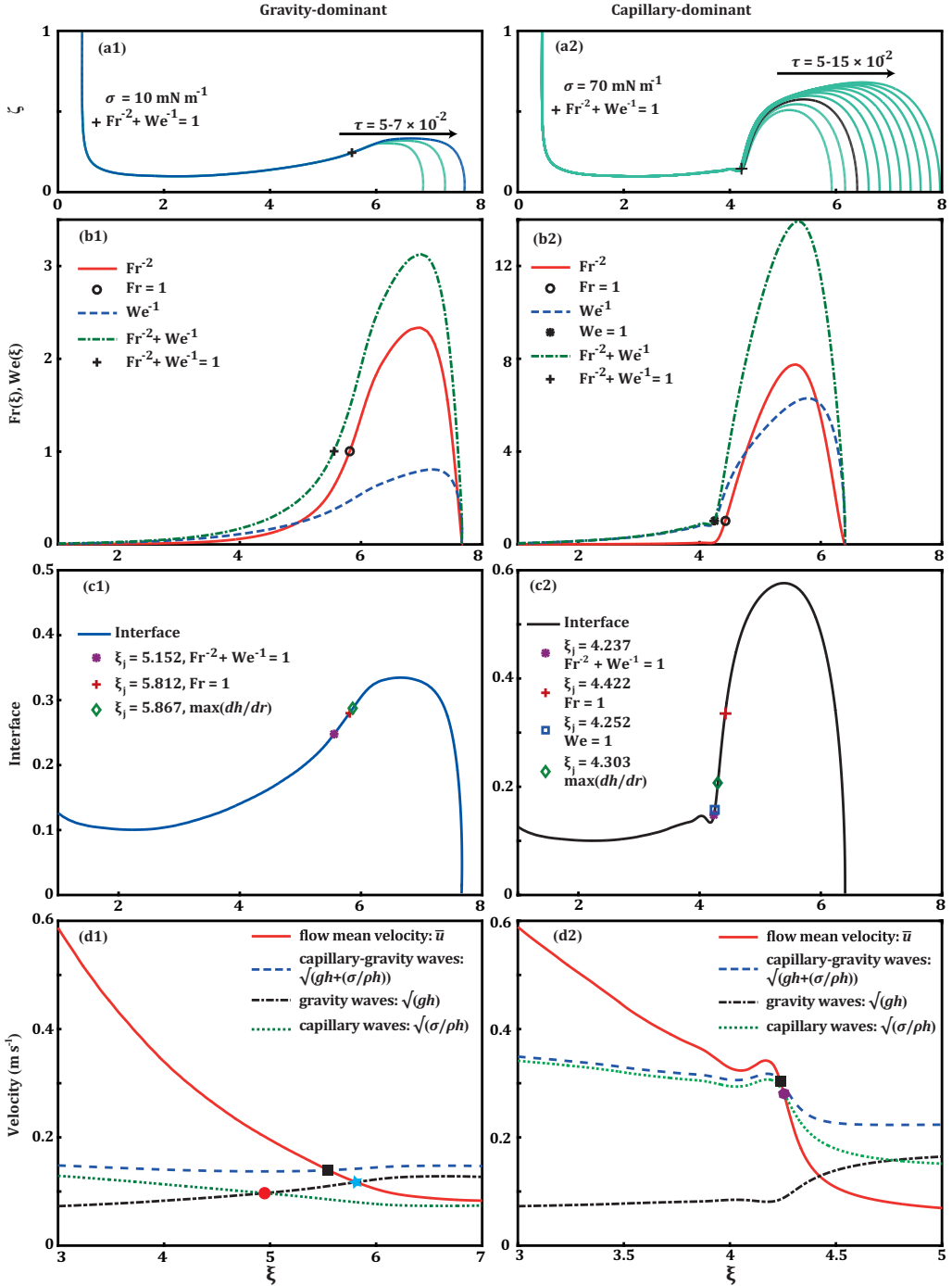
FIG. 5. Formation of a CHJ in gravity-dominant (left column) and in capillary-dominant (right column) regimes. (a) Initial formation of a CHJ showing a constant position for the jump, before the flow reaches the outlet boundary. (b) Distributions of the inverse Weber number and the Froude number squared, and that of $Fr^{-2} + We^{-1}$ before (supercritical flow) and after (subcritical flow) the jump position at $\tau = 7 \times 10^{-2}$. (c) Jump position ($\xi_j = R_j/D$) based on the conditions $Fr = 1$, $We = 1$, $Fr^{-2} + We^{-1} = 1$ or where dh/dr has its maximum. (d) Gravity ($\sqrt{gh}$), capillary ($\sqrt{\sigma/\rho h}$), and capillary-gravity ($\sqrt{gh + \sigma/\rho h}$ waves velocities before and after the jump at $\tau = 7 \times 10^{-2}$.

TABLE I. Simulation parameters. The nozzle diameter is $D = 5$ mm for all cases.

Figure	ρ (g cm^{-3})	ν (cSt)	Q (ml s^{-1})	g (m s^{-2})	σ (mN m^{-1})
5, 6	1.11	10	30	9.81	Variable
7, 12(a)	1.11	Variable	30	9.81	45
8, 12(b)	1.11	10	Variable	9.81	45
9, 13(a)	1.11	10	30	9.81	Variable
10, 13(b)	1.11	10	30	Variable	45
11, 12(c)	Variable	10	30	9.81	45
14(a)	1.11	Variable	30	9.81	45

Bhagat *et al.* [2]. The RMS percentage of applying the theoretical and experimental coefficients is about 6% and 10%, respectively.

Figure 6(b) depicts the approximate boundaries for pure capillary and gravity waves in water according to the study by Hansen *et al.* [18]. These boundaries can be obtained by neglecting the role of gravity or surface tension in the dispersion relation of capillary-gravity waves (for more details see Appendix B in Ref. [18]). As Fig. 6(b) shows, both gravity and capillary waves can be important in shallow water. Therefore, to study thin liquid film flows, it is necessary to clarify which regime dominates the flow. For instance, shallow-water gravity waves dominate the flow for frequencies lower than 5 Hz. For frequencies more than 30 Hz, the waves are essentially of capillary type. The flows measured by Bhagat *et al.* [2] have been in a capillary regime and so they did not observe gravitational effects on developing jumps.

A comparison between gravity, capillary, and capillary-gravity wave velocities is presented in the last row of Fig. 5. It shows that gravity waves overcome capillary ones in a gravity-dominant regime before the occurrence of the jump [marked with a circle in Fig. 5(d1)]. The jump position has been highlighted with a square and calculated based on the criterion of $\mathrm{Fr}^{-2} + \mathrm{We}^{-1} = 1$, which shows the position at which the flow mean velocity equals the gravity-capillary wave velocities ($\overline{u} = \sqrt{gh + \sigma/\rho h}$, $\overline{u} = Q/2\pi rh$), which is a superposition of gravity ($\sqrt{gh}$) and capillary ($\sqrt{\sigma/\rho h}$) wave velocities. In addition, Fig. 5(d1) depicts that nowhere throughout the domain in this
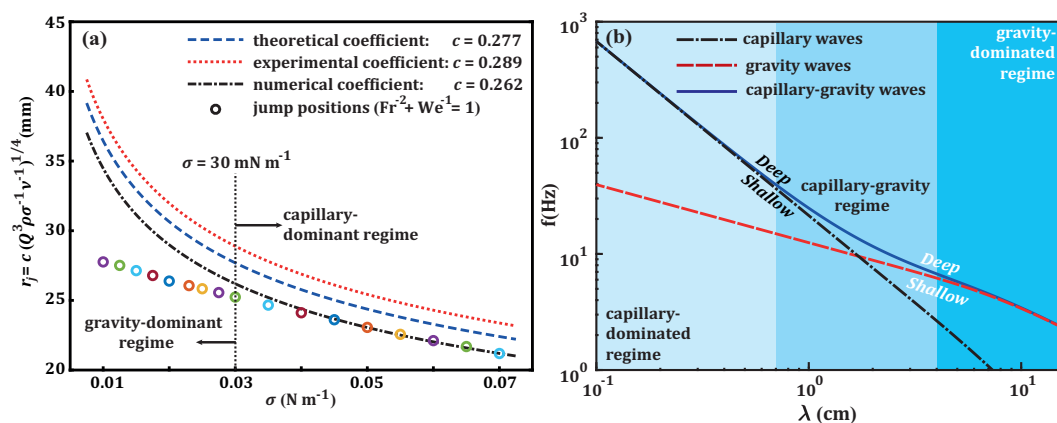

FIG. 6. (a) Possible deviations of the scaling relation of Bhagat *et al.* [2], Eq. (4), from the jump position. (b) Dispersion relation of undamped capillary-gravity waves in water. The different chromatic regions represent the approximate boundaries for pure capillary waves (small wavelengths, $\lambda < 0.7$ cm) and gravity waves (long wavelengths, $\lambda > 4$ cm). The region in the middle has mixed capillary-gravity waves. The solid line represents the relatively sharp boundary between the shallow- and deep-water limits [18].
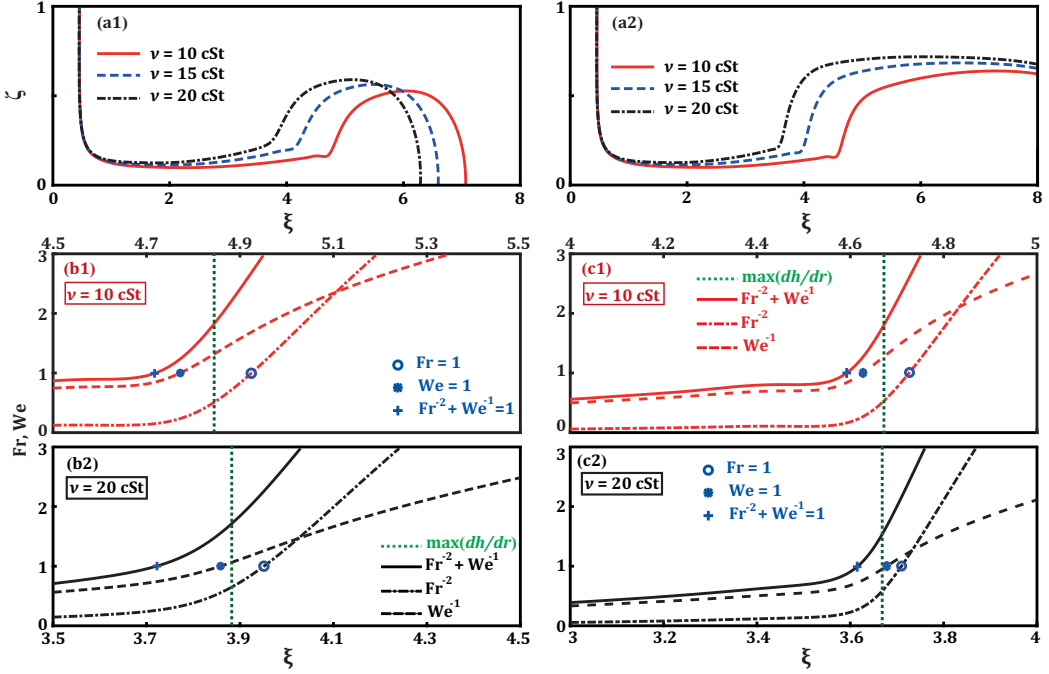
FIG. 7. Influence of viscosity on developing (left column) and developed (right column) CHJs: (a) interface geometry; (b) and (c) variation of capillary and gravity effects in the jump region.

gravity-dominant regime are the capillary wave velocities equal to the flow mean velocity to result in the critical flow condition We $= 1$. However, gravity wave velocities become equal to the mean flow velocity (highlighted with a star), which is close enough to the calculated jump position on the basis of the criterion of $Fr^{-2} + We^{-1} = 1$ to prove that the classical way of demarcating between super- and subcritical flows (Fr $= 1$) can be applied for developing CHJs in a gravity-dominant regime. Hence, gravity plays a profound role in the origin of CHJs, showing that depriving the role of gravity in the origin of CHJs is not unconditionally true. However, Fig. 5(d2) depicts the minor contribution of gravity waves to positioning a developing jump in a capillary-dominated regime.

B. Developing versus developed CHJs

This section is allocated to clarifying the influences of the outlet boundary condition on the jump. In this regard, the developing jump is compared with the developed one. Figures 7 to 11 present simulation results for both types of the CHJ combined with a variation of the most significant parameters (viscosity, volume flow rate, surface tension, gravity, and density). The simulation parameters for each case are given in Table I. It should be noted that a 90° contact angle, as mentioned in Sec. II B, is applied for simulations of developing jumps. Since Bhagat *et al.* [2] observed that the contact angle has a negligible effect on developing jumps, we restrict ourselves to the consideration of a constant contact angle.

To have a better understanding of the influence of every single parameter on gravitational and surface tension effects, the results are not presented on the basis of dimensionless numbers. For instance, an increase in the volume flow rate leads to the higher Reynolds and Weber numbers. Since the flow becomes thinner for a higher Reynolds number, stronger capillary effects could be expected. However, a higher Weber number decreases those effects on the jump.
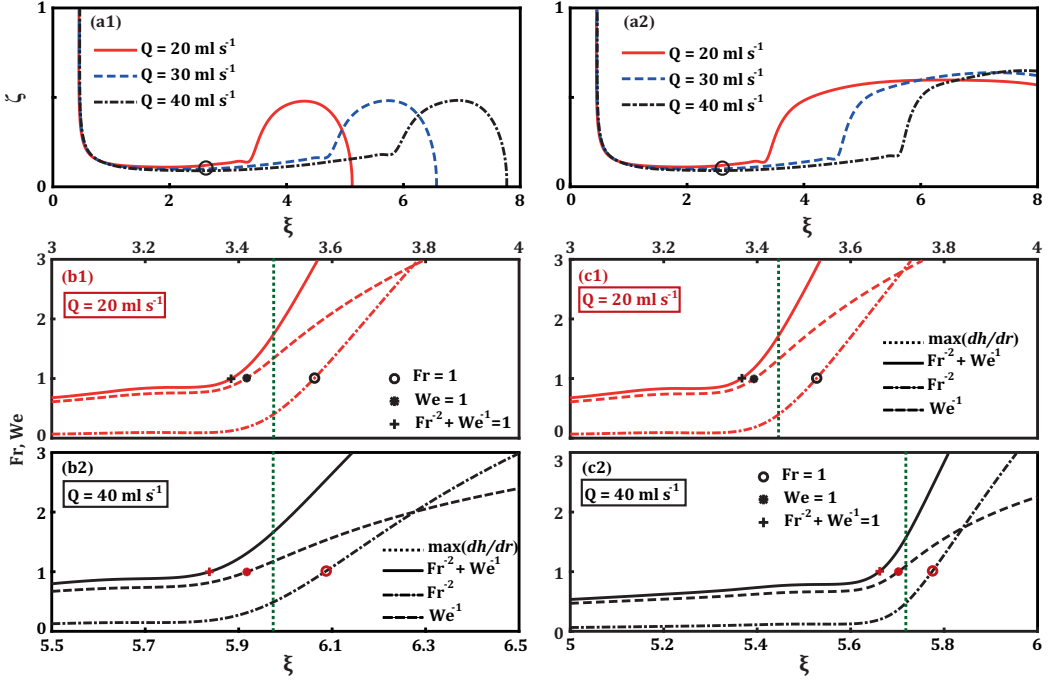
FIG. 8. Influence of volume flow rate on developing (left column) and developed (right column) CHJs: (a) interface geometry; (b) and (c) variation of capillary and gravity effects in the jump region.

1. Viscosity

The top row in Fig. 7 indicates the profound role of viscosity in the positioning of both a developing (left column) and a developed (right column) CHJ. Increasing viscosity for the same volume flow rate results in an earlier (upstream) decrease in the flow velocity and thus an increase in the film thickness. This in turn increases the velocity of gravity waves and their influence on the formation of the jump, as can be seen by comparing the distributions of We^{-1} and Fr^{-2} in Fig. 7(b1) with that of in Fig. 7(b2) for a developing CHJ. For a developed CHJ, such a comparison is provided in Figs. 7(c1) and 7(c2). For both cases, a higher viscosity increases the distance between the jump positions obtained from the criteria $We = 1$ and $Fr^{-2} + We^{-1} = 1$. Moreover, the location of the highest interfacial gradient becomes a bit closer to the jump position ($Fr^{-2} + We^{-1} = 1$) as viscosity increases in the case of a developed jump. For a developing jump, however, dh/dr becomes a bit farther from the jump position ($Fr^{-2} + We^{-1} = 1$) for a higher viscosity.

2. Volume flow rate

Influence of the volume flow rate on developing and developed jumps is presented in the left and right columns of Fig. 8, respectively. Position of the jump noticeably changes with a change in the volume flow rate. At the same comparable position in the supercritical flow upstream the jump [marked with a circle in Figs. 8(a1) and 8(a2)], the velocity of gravity waves decreases for a higher volume flow rate, because the flow thickness decreases. Nevertheless, the flow is thicker for a higher volume flow rate just before the occurrence of the jump. It means that capillary effects are decreased in the jump region for a higher volume flow rate, despite their increase in the supercritical region. This is shown in Figs. 8(b) and 8(c), where as can be seen the distance between the distributions of We^{-1} increases from that of $Fr^{-2} + We^{-1}$ for a higher volume flow rate. Notably, the effect of
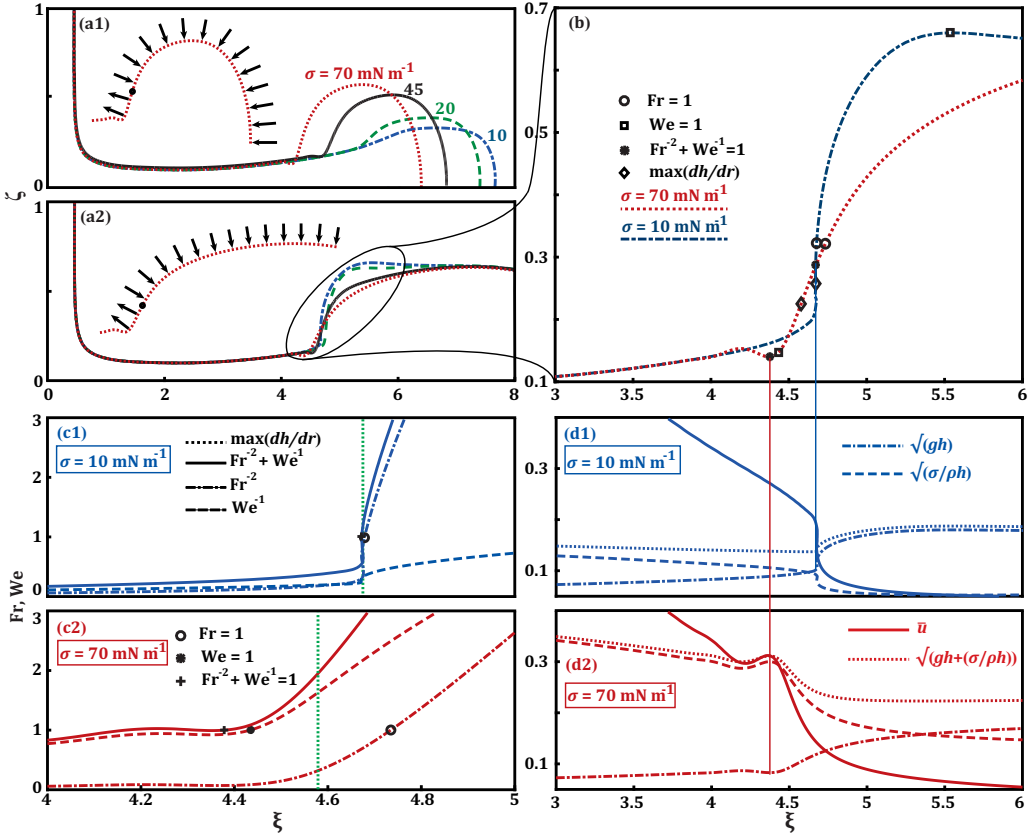
FIG. 9. Surface tension effects on the formation of CHJs: interface geometry for a developing (a1) and a developed (a2 and b) CHJ; (c) local variation of the inverse Froude number squared, the inverse Weber number, and that of $Fr^{-2} + We^{-1}$ in capillary- ($\sigma = 70$ mN m^{-1}) and gravity-dominated ($\sigma = 10$ mN m^{-1}) flow regimes for a developed jump; (d) gravity waves ($\sqrt{gh}$), capillary waves ($\sqrt{\sigma/\rho h}$), gravity-capillary waves ($\sqrt{gh + \sigma/\rho h}$), and the mean flow ($\bar{u}$) velocities for a developed jump.

higher volume flow rate on the maximum of dh/dr is similar to the effect of higher viscosity on it, because both lead to the increase in gravitational effects in the jump region.

3. Surface tension

As Fig. 9 shows, influence of the surface tension on a developing jump is stronger than on a developed one. For a developing jump, in contrast to a developed one, surface tension forces considerably act against momentum and contribute noticeably to satisfy the critical flow condition at the jump, which is schematically shown in the insets of Fig. 9(a). Since the flow downstream of the jump has not yet reached the outlet boundary, it has a rim bulb shape, which is enlarged by increasing the surface tension [Fig. 9(a1)]. Hence, the inverse pressure gradient is increased and shifts the jump position upstream. For a developed jump, on the other hand, increasing surface tension does not lead to any noticeable variation of the flow thickness downstream of the jump [Fig. 9(a2)], where the height of the flow is already formed and the influence of the surface tension is only on the smoothness of the interface in the jump region. It means, for a developing jump, that higher surface tension leads to the earlier (upstream) satisfaction of the critical flow condition and consequently to the earlier occurrence of the jump as is presented in Fig. 9(a1). On the other hand,

Fig. 9(a2) indicates that variation of the surface tension results in a minor change in the position of a developed jump.

Nevertheless, the interface profile of a developed jump is still affected by variation of the surface tension, where a significant capillary wave occurs just before the jump by increasing the surface tension [Fig. 9(b)]. A same behavior can be seen for a developing jump [Fig. 5(c)]. Simplifying the critical flow condition from $Fr^{-2} + We^{-1} = 1$ to $Fr = 1$ and/or to $We = 1$ depends on the strength of this wave. Similar to a developing jump (right column of Fig. 5), the presence of this wave in a capillary-dominant regime [$\sigma = 70$ mN m^{-1} in Fig. 9(b)] shows that the assumption of Bhagat *et al.* [2], $We = 1$, is quite a good approximation to locate the jump, because the velocity of capillary waves is very close to the velocity of gravity-capillary waves [Fig. 9(d2)]. However, the disappearance of such a capillary wave in a regime dominated by gravitational effects [$\sigma = 10$ mN m^{-1} in Fig. 9(b)] leads to the detachment of We^{-1} from $Fr^{-2} + We^{-1}$ [Fig. 9(c1)]. In such a case, the assumption of $We = 1$ poorly projects the jump position [Fig. 9(b)], and the estimated jump radius based on $Fr = 1$ is highly accurate, because the velocity of gravity waves overcomes that of capillary ones just before the occurrence of the jump [Fig. 9(d1)].

It should be noted that the highest interfacial gradient, dh/dr, accurately predicts the position of a developed jump in a gravity-dominated regime [Fig. 9(c1)]; however, its prediction becomes worse for a capillary-dominated regime [Fig. 9(c2)]. This is contrary to a developing jump, where the maximum value of dh/dr is closer to the jump position if the flow regime is capillary dominated [Fig. 5(c)].

Another aspect is the smoother interface profile of a developing jump for lower surface tension [Fig. 9(a1)]. Since a higher surface tension causes higher capillary forces trying to minimize the interface (as discussed in Sec. III A), the downstream height thickens, which yield a steeper jump profile. For a developed jump, however, Fig. 9(a2) shows that a lower surface tension yields to a steeper interface in the jump region, which goes down to the lower magnitude of surface tension forces compared to pressure forces in the jump region.

4. Gravity

Comparison of Fig. 9(a) with Fig. 10(a) indicates that the response of CHJs to the variation of gravity is in contrast to the variation of surface tension. The reason is the different functionality of surface tension forces before and after the arrival of the flow at the outlet boundary, which is schematically shown in the insets of Fig. 9(a). In fact, the net of surface tension forces along with viscous forces cause an inverse pressure gradient that compensates the momentum of the flow at the jump. Although lower gravity decreases the inverse pressure gradient, this effect is negligible for developing jumps in comparison to the effects of surface tension and viscous forces. Hence, for the same surface tension, lowering gravity slightly shifts the jump position [Figs. 10(a1) and 10(b1)]. However, for a developed jump, the net of surface tension forces loses a considerable portion of its opposition to the momentum of the flow, and the role of inverse pressure gradient in positioning the jump becomes quite significant. Therefore, reducing gravity for a developed CHJ considerably moves the jump position downstream [Figs. 10(a2) and 10(b2)], which is inconsistent with previous findings [40–42].

This downstream movement of developed jumps by decreasing gravity means that the jump in general becomes weaker, since a lower amount of momentum is dissipated, which results in a smoother interface profile in the jump region. Such a downstream movement of the jump by decreasing gravity can cause the disappearance of the jump in a developed case [41]. For a developing jump, on the other hand, reducing gravity does not lead to a considerable downstream movement of the jump position. It means that the same amount of momentum is dissipated through a developing jump, despite the variation of gravity. The reason lies in the fact that the flow regime is more sensitive to the variation of surface tension than that of gravity. Nevertheless, the interface profile of a developing jump changes with gravity and becomes steeper in the jump region for lower
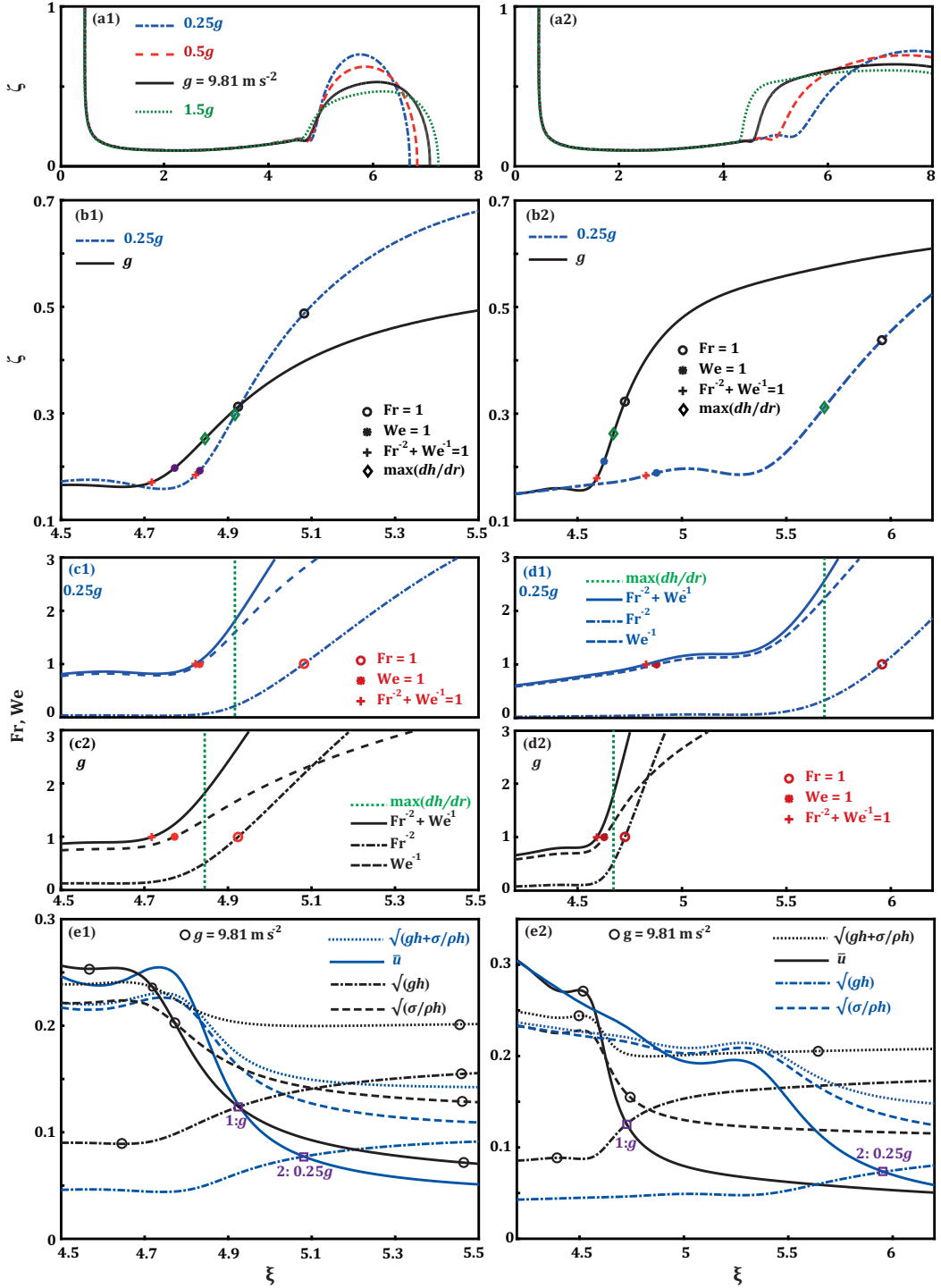
FIG. 10. Gravity effects on the formation of a developing (left column) and a developed (right column) CHJ: (a) and (b) interface geometry; (c) and (d) local variation of the inverse Froude number squared, the inverse Weber number, and that of $Fr^{-2} + We^{-1}$; (e) gravity waves ($\sqrt{gh}$), capillary waves ($\sqrt{\sigma/\rho h}$), gravity-capillary waves ($\sqrt{gh + \sigma/\rho h}$), and the mean flow ($\bar{u}$) velocities.

gravitational accelerations. The reason is the reinforcement of capillary effects in the jump region by decreasing gravity, which causes to a larger droplet-shape fluid bulb.

The weaker gravitational effects are accompanied by a stronger capillary wave just before both a developing [Fig. 10(b1)] and a developed [Fig. 10(b2)] CHJ. The stronger capillary wave is intertwined with the enhancement of capillary effects on the jump. This is given in Fig. 10(c) for a developing and in Fig. 10(d) for a developed jump, where the distribution of We^{-1} overlaps that of $\mathrm{Fr}^{-2} + \mathrm{We}^{-1}$. Consequently, the distance between the projected jump positions based on the critical flow conditions $\mathrm{Fr} = 1$ and $\mathrm{Fr}^{-2} + \mathrm{We}^{-1} = 1$ is increased as gravity decreases for both a developing [Fig. 10(c1)] and a developed Fig. 10(d1)] jump.

It should be noted that the maximum value of dh/dr does not experience a considerable change for developing jumps as gravity varies [Figs. 10(c1) and 10(c2)]. This is different for developed jumps [Figs. 10(d1) and 10(d2)]. Figure 10(d1) shows that the smoothness of the interface for low gravity moves the location of the maximum value of dh/dr away from the jump position.

Another point is that the supercritical flow thickness upstream of the jump is not affected by the variation of gravity [Fig. 10(a)]. Hence, the capillary wave velocities, $\sqrt{\sigma/\rho h}$, almost remain unchanged and overlap each other upstream the jump for both a developing [dashed lines in Fig. 10(e1)] and a developed [dashed lines in Fig. 10(e2)] jump. Nevertheless, higher gravity increases the capillary-gravity wave velocities ($\sqrt{gh + \sigma/\rho h}$), which is mainly due to the increase in gravity wave velocities ($\sqrt{gh}$). The marked positions 1 and 2 in Figs. 10(e1) and 10(e2) correspond to the locations where the mean velocity of the wall-jet equals gravity wave velocities ($\mathrm{Fr} = 1$) for a high (g) and a low $\frac{1}{4}g$ gravitational acceleration, respectively. It shows that the critical flow condition of $\mathrm{Fr} = 1$ is not applicable to determine the jump position in low-gravity mediums (capillary-dominated regimes) for both a developing and a developed jump.

5. Density

Variation of the density affects inertia forces which are balanced out at the jump through the net of gravitational, viscous, and surface tension forces. Since the thickness of the supercritical flow upstream of the jump undergoes no changes through the variation of the density in both a developing and a developed CHJ [Fig. 11(a)], gravitational effects remain unchanged before the jump. This fact can be observed in Fig. 11(e), where gravity wave velocities overlap each other in the upstream region (see dashed-dotted lines). For a constant kinematic viscosity (see Table I for Fig. 11) and an unchanged height of the flow in the supercritical region, viscous forces do not face any noticeable change by the variation of the density as well. Hence, it is expected that variations of the density mainly affect surface tension forces.

The second row in Fig. 11 shows the intensification of capillary effects by decreasing the density. As a result, a significant capillary wave prior to the jump appears that makes the assumption of $\mathrm{We} = 1$ applicable to accurately predict the jump position for both a developing and a developed jump [Fig. 11(b)] in low-density free-surface liquid jets. Nevertheless, the sudden rise of the interface in the jump region of a developing jump results in the quick augmentation of gravitational effects for low densities. Therefore, the predicted position of a developing jump by applying the critical flow condition of $\mathrm{Fr} = 1$ is also a relatively good approximation even though the capillary effects are intensified by decreasing the density [Figs. 11(b1) and 11(c1)]. For a developed jump, however, $\mathrm{Fr} = 1$ inaccurately predicts the jump radius for low densities, because the interface profile smoothly grows, and consequently gravitational effects do not swiftly become important [Figs. 11(b2) and 11(d1)].

Since increasing the density damps capillary waves right before the jump and weakens surface tension forces [for both a developing, Fig. 11(b1), and a developed, Fig. 11(b2), jump], gravitational effects become significant and comparable to that of capillary ones. This is shown in Figs. 11(e1) and 11(e2), where the velocities of gravity and capillary waves reach the mean flow velocity at the same location. Accordingly, the obtained jump positions on the basis of $\mathrm{We} = 1$ and $\mathrm{Fr} = 1$ are the same [Figs. 11(c2) and 11(d2)]. For a developed jump, high densities result in an instantaneous
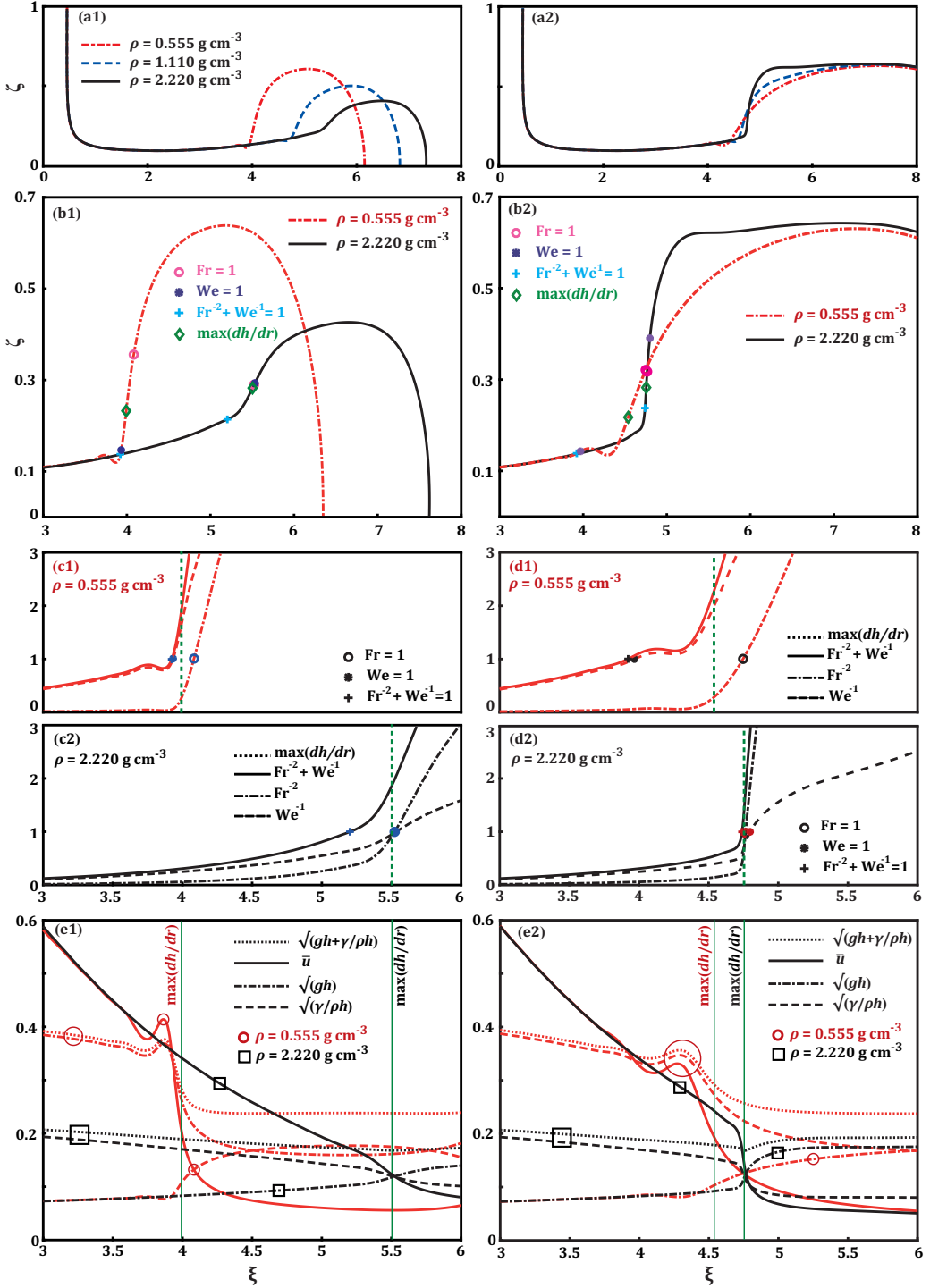
FIG. 11. Influence of density on the formation of a developing (left column) and a developed (right column) CHJ: (a) and (b) interface geometry; (c) and (d) local variation of the inverse Froude number squared, the inverse Weber, and that of $\mathrm{Fr}^{-2} + \mathrm{We}^{-1}$; (e) gravity waves ($\sqrt{gh}$), capillary waves ($\sqrt{\sigma/\rho h}$), gravity-capillary waves ($\sqrt{gh + \sigma/\rho h}$), and the mean flow ($\overline{u}$) velocities.

increase of the flow thickness at the jump that promptly intensifies gravitational effects [Fig. 11(d2)]. Hence, the assumption of Fr = 1 works well to obtain the jump position.

In addition, the maximum value of dh/dr is accurate enough to be considered as the jump position for high-density (gravity-dominated) liquid jets in a developed case [Fig. 11(e2)]. In a developing case, predictions of dh/dr are more precise for low-density (capillary-dominated) liquid jets [Fig. 11(c1)].

C. Scaling analysis

It was shown that the scaling relation of Bhagat *et al.* [2], Eq. (4), will result in considerable deviations from the position of developing jumps if the flow regime is gravity dominated [Fig. 6(a)]. In addition, Bohr's model, Eq. (2), was presented for developed CHJs, but for cases in which the jump occurs of its own accord and without forcing it to circumvent an obstacle. In this section, a generalized scaling relation for the jump radius is presented which holds up in both gravity- and capillary-dominant regimes not only for a developing, but also for a developed, CHJ. The key point in this regard is the consideration of both gravity and capillary waves in the critical flow condition. Therefore, adding gravity to the scaling analysis of Bhagat *et al.* [2] yields the following dimensionless parameters for the vertical impingement of a round free-surface liquid jet upon a horizontal plate shown in Fig. 1 (note that in this subsection α stands for the dimensionless flow thickness):

$$\text{Re} = \frac{\overline{u}h}{\nu}, \quad \text{We} = \frac{\rho\overline{u}^2 h}{\sigma}, \quad \text{Fr}^2 = \frac{\overline{u}^2}{gh}, \quad \alpha = \frac{h}{R_j}. \tag{10}$$

The assumption of balancing the radial flow by viscous drag at the jump, $\overline{u}/R_j \sim \nu/h^2$, implies $\alpha\text{Re} = O(1)$ [2]. Then depriving the role of gravity of being important in the origin of CHJs (setting g equal to zero in $\text{Fr}^{-2} + \text{We}^{-1} = 1$) and consequently applying the critical flow condition of We = 1 at the jump result in the scaling relation of Eq. (4) [2]. On the other hand, neglecting the surface tension in the critical flow condition of $\text{Fr}^{-2} + \text{We}^{-1} = 1$ and keeping gravity (in other words, applying Fr = 1 as the critical flow condition) lead to the scaling relation of Bohr *et al.* [4], Eq. (2). Considering both gravity and surface tension by applying $\text{Fr}^{-2} + \text{We}^{-1} = 1$ as the critical flow condition together with the continuity equation, $q = Q/2\pi = R_j h\overline{u}$, and retaining the assumption of $\alpha\text{Re} = O(1)$ result in the following system of equations for the flow thickness, local mean flow velocity, and jump radius:

$$h = \frac{R_j^2 \nu}{q}, \quad R_j = \frac{\overline{u}h^2}{\nu}, \quad \overline{u}^2 = gh + \frac{\sigma}{\rho h}. \tag{11}$$

Combination of the above set of equations in terms of the jump radius (R_j) yields

$$g\left(\frac{\nu}{q}\right)^5 R_j^8 + \frac{\sigma}{\rho}\left(\frac{\nu}{q}\right)^3 R_j^4 - \nu^2 = 0. \tag{12}$$

The above equation can be solved to obtain the following generalized scaling relation:

$$\frac{R_j}{R_0} = c, \quad R_0 = \left(\frac{\sigma}{2g\rho}\left(\frac{q}{\nu}\right)^2\left\{-1 + \left[1 + 4\nu qg\left(\frac{\rho}{\sigma}\right)^2\right]^{\frac{1}{2}}\right\}\right)^{\frac{1}{4}}, \quad q = \frac{Q}{2\pi}. \tag{13}$$

Accordingly, Figs. 12 and 13 present the predictions of Eq. (2), $R_j = c(q^5\nu^{-3}g^{-1})^{1/8}$, Eq. (4), $R_j = c(q^3\rho\,\nu^{-1}\sigma^{-1})^{1/4}$, and that of the generalized scaling relation, Eq. (13), for the radius of a developing (left columns) and a developed jump (right columns). For a developing jump (left columns in these figures), it can be seen that applying the fixed constant coefficient of $c = 1.081$ in Eq. (13) results in the more accurate predictions for the jump radius in comparison to the predictions of Eqs. (2) and (4). Notably, Eq. (4) properly estimates the position of a developing jump
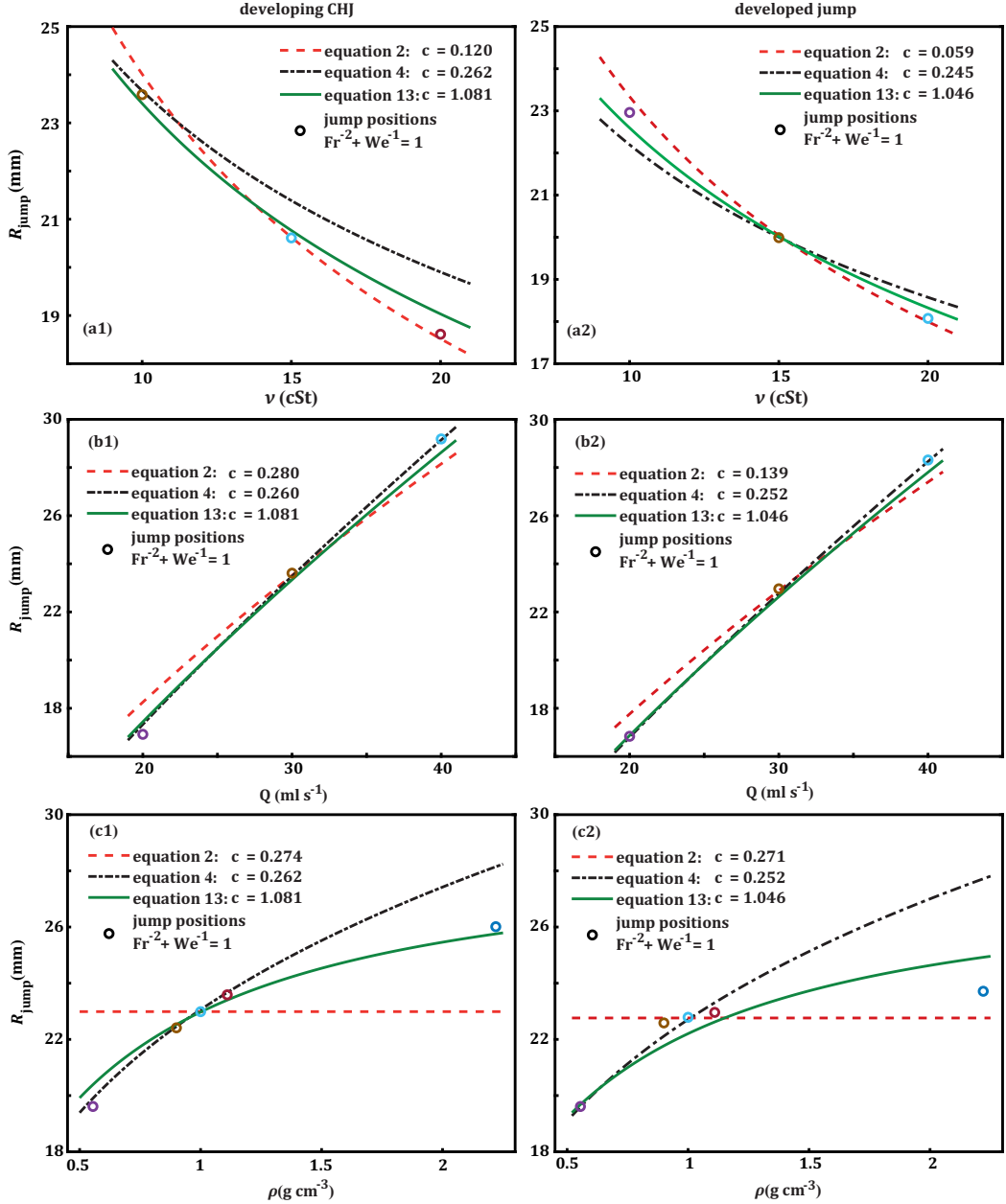
FIG. 12. Comparisons between the jump positions predicted by $R_j = c(q^5\nu^{-3}g^{-1})^{1/8}$ [Eq. (2)] and $R_j = c(q^3\rho\,\nu^{-1}\sigma^{-1})^{1/4}$ [Eq. (4)] and Eq. (13) in terms of viscosity (a), volume flow rate (b), and density (c) for the developing (left column) and developed (right column) CHJs.

applying $c = 0.262$, except when gravity effects dominate capillary ones. For instance, increasing the viscosity [Fig. 12(a1)], increasing the density [Fig. 12(c1)], or decreasing the surface tension [Fig. 13(a1)] leads to the attenuation of capillary waves, and consequently to the propulsion of the flow regime toward being gravity dominated. It should be noted that the maximum error of Eq. (4) lies under 4% for predicting the position of a developing jump in a capillary-dominant
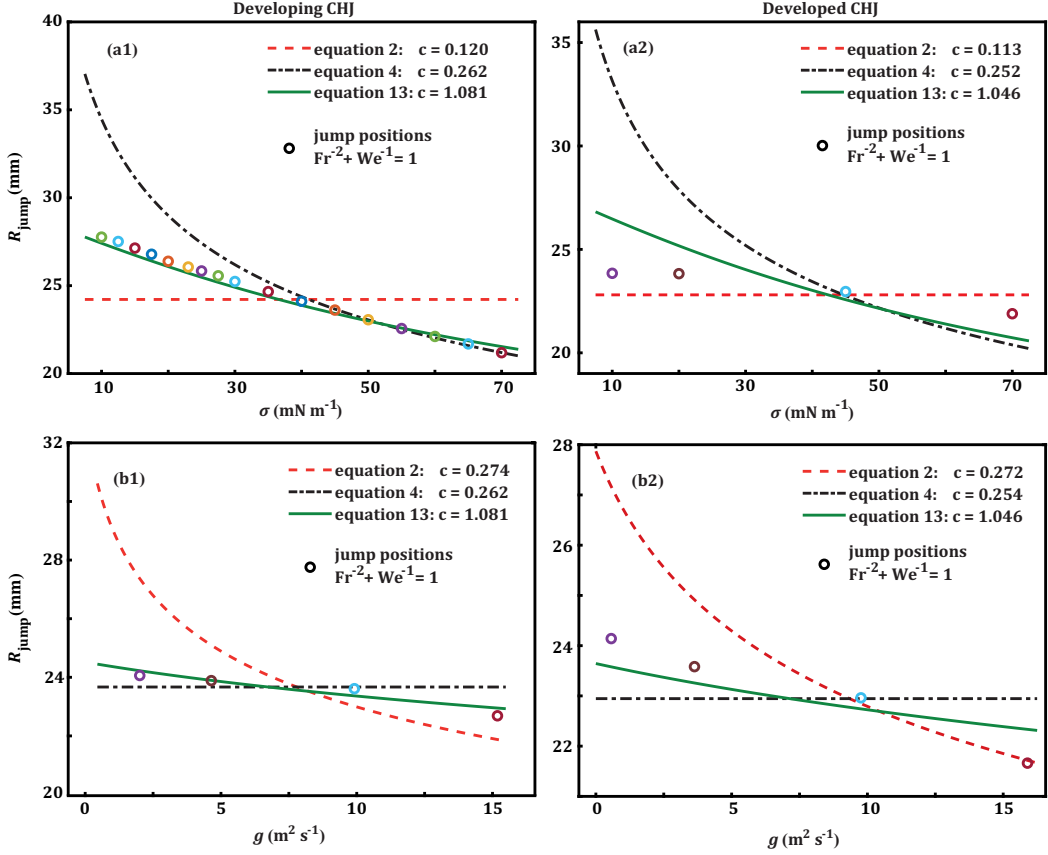
FIG. 13. Comparisons between the jump positions predicted by $R_j = c(q^5 \nu^{-3} g^{-1})^{1/8}$ [Eqs. (2)] and $R_j = c(q^3 \rho \nu^{-1} \sigma^{-1})^{1/4}$ [Eq. (4)] and Eq. (13) in terms of surface tension (a) and gravity (b) for the developing (left column) and developed (right column) CHJs.

regime [Fig. 13(b1)]. In a gravity-dominant regime, however, its error amounts to around 25%, as the surface tension is decreased to $\sigma = 10$ mN m^{-1} [Fig. 13(a1)]. By contrast, the maximum error of the generalized scaling relation, Eq. (13), for predicting the position of a developing jump is around 1% irrespective of the flow regime. It can be also seen that the predictions of Eq. (2) for the radius of a developing CHJ are inaccurate, especially with the variation of the gravitational acceleration [Fig. 13(b1)]. The reason is that the gravitational acceleration is scaled with the power of 1/8 in Eq. (2), whereas it carries less weight in the positioning of a developing jump when the flow regime is capillary dominant. Hence, Eq. (2) is not a proper choice to predict the position of a developing jump.

For developed jumps created by forcing the flow to circumvent an obstacle (right columns in Figs. 12 and 13), neither Eq. (2) nor Eq. (4) can accurately predict the jump position. Nevertheless, the predictions of Eq. (4) are more or less acceptable, although it has not been inherently applied to a developed jump. Deviations of the predictions of Eq. (4) from the position of developed jumps can be observed when the flow is dominated by gravity effects (Figs. 12(c2) and 13(a2)]. In addition, the effects of a variation in the surface tension on the position of a developed jump are overestimated through applying Eq. (4) [Fig. 13(a2)], and the effects of a variation in the gravitational acceleration on the position of a developed jump are not just included in Eq. (4) [Fig. 13(b2)].
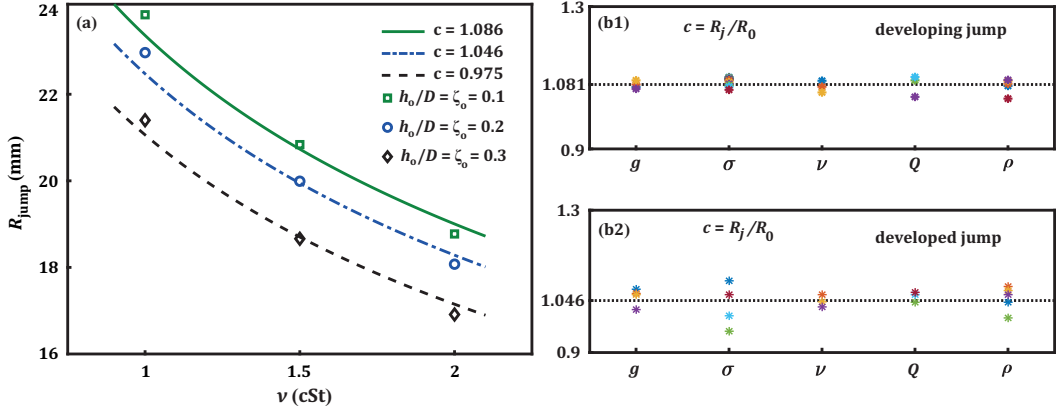
FIG. 14. (a) Influence of the obstacle height on the jump position and on the scaling relation of Eq. (13); (b) evaluation of the constant coefficient of Eq. (13) for the developing (b1) and developed (b2) jumps.

Equation (2), which has been essentially obtained for developed jumps (Bohr *et al.* [4]), requires different constant coefficients to yield proper approximations for the radius of developed jumps, although the height of the obstacle remains constant, as is shown in the right columns of Figs. 12 and 13. Moreover, variation of the density is not included in Eq. (2), which causes incorrect predictions for the jump position in low-density free-surface liquid jets [Fig. 12(c2)], where capillary effects are intensified and cause the appearance of a relatively strong capillary wave right before the jump [see Fig. 11(b2)]. The absence of the surface tension in Eq. (2), however, does not lead to a considerable deviation of its predictions from the radius of developed jumps [Fig. 13(a2)]. The reason is that surface tension forces act to a small degree against momentum once the flow arrives at the outlet boundary, because the downstream thickness of the flow is high and gravitational effects dominate the flow. Therefore, an increase in surface tension no longer changes the height of the free surface as it affects the free surface in the case of a developing jump, where a progressive interface approaches the outlet boundary [compare the insets of Figs. 9(a1) and 9(a2)].

In contrast to the scaling relations of Bohr *et al.* [4] [Eq. (2)] and Bhagat *et al.* [2] [Eq. (4)], Eq. (13) shows that it can be applied to appropriately estimate the position of both a developing and a developed jump for a wide range of liquids and laminar flow conditions. More importantly, it can be seen that its constant coefficient, in contrast to the constant coefficients of Eqs. (2) and (4), does not depend on the variation of the fluid properties.

1. The influence of obstacle height on the scaling relation

The obstacle height, which applies for the developed jumps, considerably affects the jump by increasing the flow thickness downstream of the jump and consequently by increasing gravitational effects. It is a controlling factor not only to locate the jump, but also arguably to change the flow structure in the hydraulic jump region [16]. To illustrate whether the scaling relation of Eq. (13) depends on the height of the obstacle, Fig. 14(a) is provided showing the change of the jump position with viscosity for different heights of the obstacle. The corresponding simulation parameters are provided in Table I. For each obstacle height a specific constant is necessary to be applied in the scaling relation of Eq. (13). The resulting parallel curves for different obstacle heights indicate that the scaling of viscosity in Eq. (13) does not depend on the height of the obstacle. The same conclusion can be drawn for the other parameters in Eq. (13) as well.

2. Evaluation of the constant coefficient of the scaling relation

To determine the constant coefficient of Eq. (13), Fig. 14(b) is provided, which shows the variation of the dimensionless jump radius with all the involved parameters. As can be seen,

numerical results collapse on to the line $R_j/R_0 = 1.081 \pm 0.035$ for a developing jump [Fig. 14(b1)] and on to the line $R_j/R_0 = 1.046 \pm 0.122$ for a developed one [Fig. 14(b2)] with the dimensionless obstacle height of $\zeta_o = h_o/D = 0.2$ over the entire range calculated ($381.972 < \mathrm{Re}_i < 1.186 \times 10^3$, $127.962 < \mathrm{We}_i < 1.296 \times 10^3$, $5.633 < \mathrm{Fr}_i < 13.798$). The subscript i indicates the entrance values to the medium. Note that the nozzle diameter is the characteristic length for calculating the inlet Froude number [19].

IV. CONCLUSIONS

This study scrutinizes the formation of circular hydraulic jumps (CHJs) in two cases, before and after the arrival of the flow at the outlet boundary, trying to find out whether gravity plays any role in both the initial [developing jump, Fig. 1(a)] and the final formation [developed jump, Fig. 1(b)] of the jump. Numerical results coherently show the presence of two kinds of flow regimes in the formation of the CHJ: the gravity- and the capillary-dominated regimes. The governing flow regime is more sensitive to the variation of the surface tension rather than to the gravitational acceleration. Nevertheless, the role of gravity in the formation and origin of the jump cannot be neglected. If the flow regime is capillary dominant, a variation in the gravitational acceleration will slightly affect developing CHJs [Fig. 13(b1)]. This is consistent with the study by Bhagat *et al.* [2], where the role of gravity was observed to be of minor importance in the initial formation of the jump. However, when gravitational effects dominate the flow, which occurs for low surface tensions (Fig. 5, left column), the role of gravity in the initial formation of developing CHJs becomes quite significant [Fig. 6(a) and Fig. 13(a1)].

A developed CHJ, on the other hand, is more sensitive to the variation of gravity [Fig. 10(a2)] rather than surface tension [Fig. 9(a2)]. As long as the flow has not yet reached the outlet boundary (in a developing jump), surface tension forces build a rim bulb flow around the jump approaching the outlet boundary [see the inset of Fig. 9(a1)]. Therefore, increasing the surface tension will enlarge this rim bulb flow and will consequently decrease the jump radius [Fig. 9(a1)]. Once the flow arrives at the outlet boundary and a developed jump is formed, variation of the surface tension affects the smoothness of the interface in the jump region and not the position of the jump, because the height of the flow downstream of the jump is already formed and a progressive interface is no longer exists that could be enlarged by an increase in the surface tension [see the inset of Fig. 9(a2)]. In such a case, gravitational effects become quite important that strongly depend on the height of the downstream flow, and this height remains constant with a variation in surface tension.

The effects of other important parameters such as viscosity, volume flow rate, and density on a developing and a developed CHJ are also presented. Variation of these parameters leads to the intensification/abatement of capillary/gravitational effects. A decrease of capillary effects occurs by increasing the viscosity, the density, or the gravitational acceleration and by decreasing the surface tension. The assumption of $\mathrm{Fr} = 1$ to locate the jump is applicable when capillary effects are decreased. By contrast, the critical flow condition $\mathrm{We} = 1$ can be applied instead of the superposition of capillary and gravitational effects $\mathrm{Fr}^{-2} + \mathrm{We}^{-1} = 1$ only if the flow regime is capillary dominant. When the orders of significance of capillary and gravitational forces are the same, it is necessary to apply the critical flow condition of $\mathrm{Fr}^{-2} + \mathrm{We}^{-1} = 1$ for obtaining the jump position. The location of the highest interfacial derivation of the flow thickness, dh/dr, shows in most cases to be a good approximation for the jump position. In particular, its predictions become more accurate as the flow regime tends to be gravity dominated in developed jumps and to be capillary dominated in developing jumps.

The scaling relation presented by Bhagat *et al.* [2] works well to predict the position of developing jumps in capillary-dominant regimes, which is improved here to be applicable for gravity-dominated flow regimes as well. In this regard, a generalized scaling relation is obtained considering both capillary and gravity effects through applying $\mathrm{Fr}^{-2} + \mathrm{We}^{-1} = 1$ as the critical flow condition. The resulted generalized scaling relation shows quite a good accuracy to predict the jump position in both capillary- and gravity-dominant regimes. Moreover, it projects the radius of a

developed CHJ more precisely than the available scaling relations of this kind. It is found that the obstacle height affects only the constant coefficient of this generalized scaling relation and does not change the scaling of fluid properties.

An important continuation of this work would be the investigation of the claim made by Duchesne *et al.* [20] for the critical flow condition $\alpha^2 \mathrm{We}^{-1} + \mathrm{Fr}^{-2} = 1$ instead of $\mathrm{We}^{-1} + \mathrm{Fr}^{-2} = 1$. The latter one was thoroughly investigated here. A detailed comparison between the applicability of these two critical flow conditions with the aid of numerical simulations will be our next study in this field.

[1] W. H. Hager, *Energy Dissipators and Hydraulic Jump* (Springer Netherlands, Dordrecht, 2010).

[2] R. K. Bhagat, N. K. Jha, P. F. Linden, and D. I. Wilson, On the origin of the circular hydraulic jump in a thin liquid film, J. Fluid Mech. **851**, 11 (2018).

[3] E. J. Watson, The radial spread of a liquid jet over a horizontal plane, J. Fluid Mech. **20**, 481 (1964).

[4] T. Bohr, P. Dimon, and V. Putkaradze, Shallow-water approach to the circular hydraulic jump, J. Fluid Mech. **254**, 635 (1993).

[5] K. Yokoi and F. Xiao, Relationships between a roller and a dynamic pressure distribution in circular hydraulic jumps, Phys. Rev. E **61**, R1016 (2000).

[6] N. Rojas, M. Argentina, and E. Tirapegui, A progressive correction to the circular hydraulic jump scaling, Phys. Fluids **25**, 042105 (2013).

[7] X. Liu and J. H. Lienhard, The hydraulic jump in circular jet impingement and in other thin liquid films, Exp. Fluids **15**, 108 (1993).

[8] J. W. M. Bush and J. M. Aristoff, The influence of surface tension on the circular hydraulic jump, J. Fluid Mech. **489**, 229 (2003).

[9] B. Mohajer and R. Li, Circular hydraulic jump on finite surfaces with capillary limit, Phys. Fluids **27**, 117102 (2015).

[10] R. Fernandez-Feria, E. Sanmiguel-Rojas, and E. Benilov, On the origin and structure of a stationary circular hydraulic jump, Phys. Fluids **31**, 072104 (2019).

[11] I. Tani, Water jump in the boundary layer, J. Phys. Soc. Jpn. **4**, 212 (1949).

[12] M. Kurihara, On hydraulic jumps, Proceedings of the Report of the Research Institute for Fluid Engineering, Kyusyu Imperial University **3**, 11 (1946).

[13] T. Bohr, V. Putkaradze, and S. Watanabe, Averaging Theory for the Structure of Hydraulic Jumps and Separation in Laminar Free-Surface Flows, Phys. Rev. Lett. **79**, 1038 (1997).

[14] S. Watanabe, V. Putkaradze, and T. Bohr, Integral methods for shallow free-surface flows with separation, J. Fluid Mech. **480**, 233 (2003).

[15] K. Yokoi and F. Xiao, Mechanism of structure formation in circular hydraulic jumps: Numerical studies of strongly deformed free-surface shallow flows, Physica D **161**, 202 (2002).

[16] T. Bohr, C. Ellegaard, A. E. Hansen, and A. Haaning, Hydraulic jumps, flow separation and wave breaking: An experimental study, Physica B **228**, 1 (1996).

[17] C. Ellegaard, A. E. Hansen, A. Haaning, and T. Bohr, Experimental results on flow separation and transitions in the circular hydraulic jump, Phys. Scr. **T67**, 105 (1996).

[18] S. T. Hansen, S. Hørlück, D. Zauner, P. Dimon, C. Ellegaard, and S. C. Creagh, Geometric orbits of surface waves from a circular hydraulic jump, Phys. Rev. E **55**, 7048 (1997).

[19] Y. Wang and R. E. Khayat, The role of gravity in the prediction of the circular hydraulic jump radius for high-viscosity liquids, J. Fluid Mech. **862**, 128 (2019).

[20] A. Duchesne, A. Andersen, and T. Bohr, Surface tension and the origin of the circular hydraulic jump in a thin liquid film, Phys. Rev. Fluids **4**, 084001 (2019).

[21] C. W. Hirt and B. D. Nichols, Volume of fluid (VOF) method for the dynamics of free boundaries, J. Comput. Phys. **39**, 201 (1981).

[22] J. Brackbill, D. Kothe, and C. Zemach, A continuum method for modeling surface tension, J. Comput. Phys. **100**, 335 (1992).

[23] D. Kothe and R. C. Mjolsness, Ripple—A new model for incompressible flows with free surfaces, AIAA J. **30**, 2694 (1992).

[24] G. P. Sasmal and J. I. Hochstein, Marangoni convection with a curved and deforming free surface in a cavity, J. Fluids Eng. **116**, 577 (1994).

[25] J. R. Richards, A. M. Lenhoff, and A. N. Beris, Dynamic breakup of liquid–liquid jets, Phys. Fluids **6**, 2640 (1994).

[26] G. Wang, Finite element simulations of free surface flows with surface tension in complex geometries, J. Fluids Eng. **124**, 584 (2002).

[27] H. Jasak, Error analysis and estimation for finite volume method with applications to fluid flow, Ph.D. thesis, Imperial College, University of London, London, 1996.

[28] O. Ubbink, Numerical prediction of two fluid systems with sharp interfaces, Ph.D. thesis, Imperial College, University of London, London, 1997.

[29] H. Rusche, Computational UID dynamics of dispersed two-phase flows at high phase fractions, Ph.D. thesis, Imperial College, University of London, London, 2002.

[30] S. S. Deshpande, L. Anumolu, and M. F. Trujillo, Evaluating the performance of the two-phase flow solver interfoam, Comput. Sci. Disc. **5**, 014016 (2012).

[31] B. Lafaurie, C. Nardone, R. Scardovelli, S. Zaleski, and G. Zanetti, Modelling merging and fragmentation in multiphase flows with surfer, J. Comput. Phys. **113**, 134 (1994).

[32] W. Rohlfs and P. Pischke, Introduction and application of a smooth interface compression method in VOF (unpublished).

[33] W. Rohlfs, P. Pischke, and B. Scheid, Hydrodynamic waves in films flowing under an inclined plane, Phys. Rev. Fluids **2**, 170 (2017).

[34] W. Rohlfs, C. Ehrenpreis, H. D. Haustein, and R. Kneer, Influence of viscous flow relaxation time on self-similarity in free-surface jet impingement, Intl. J. Heat Mass Transf. **78**, 435 (2014).

[35] W. Rohlfs, M. Binz, and R. Kneer, On the stabilizing effect of a liquid film on a cylindrical core by oscillatory motions, Phys. Fluids **26**, 022101 (2014).

[36] M. Bieber, R. Kneer, and W. Rohlfs, Self-similarity of heat transfer characteristics in laminar submerged and free-surface slot jet impingement, Intl. J. Heat Mass Transf. **104**, 1341 (2017).

[37] A. Duchesne, Constant froude number in a circular hydraulic jump and its implication on the jump radius selection, Europhys. Lett. **107**, 54002 (2014).

[38] E. C. Button, J. F. Davidson, G. J. Jameson, and J. E. Sader, Water bells formed on the underside of a horizontal plate. Part 2. Theory, J. Fluid Mech. **649**, 45 (2010).

[39] J. F. Prince, D. Maynes, and J. Crockett, On jet impingement and thin film breakup on a horizontal superhydrophobic surface, Phys. Fluids **27**, 112108 (2015).

[40] C. Avedisian and Z. Zhao, The circular hydraulic jump in low gravity, Proc. R. Soc. London A **456**, 2127 (2000).

[41] M. Mathur, R. DasGupta, N. R. Selvi, N. S. John, G. U. Kulkarni, and R. Govindarajan, Gravity-Free Hydraulic Jumps and Metal Femtoliter Cups, Phys. Rev. Lett. **98**, 164502 (2007).

[42] R. Dasgupta, G. Tomar, and R. Govindarajan, Numerical study of laminar, standing hydraulic jumps in a planar geometry, Eur. Phys. J. E **38**, 45 (2015).